International Journal of Modern Physics A
Vol. 35, Nos. 34 & 35 (2020) 2044017 (13 pages)

DOI: 10.1142/S0217751X20440170

A high precision narrow-band neutrino beam: The ENUBET project

M. Torti,[1,2,*] F. Acerbi,[3,4] A. Berra,[1,16] M. Bonesini,[1] A. Branca,[5,6] C. Brizzolari,[1,2] G. Brunetti,[5] M. Calviani,[18] S. Capelli,[1,16] S. Carturan,[5,7] M. G. Catanesi,[8] N. Charitonidis,[18] S. Cecchini,[9] F. Cindolo,[9] G. Collazuol,[5,6] E. Conti,[5] F. Dal Corso,[5] C. Delogu,[5,6] G. De Rosa,[10,11] A. Falcone,[1,2] A. Gola,[3] C. Jollet,[12] V. Kain,[18] B. Klićek,[13] Y. Kudenko,[14] M. Laveder,[5,6] A. Longhin,[5,6] L. Ludovici,[15] E. Lutsenko,[1,16] L. Magaletti,[8,17] G. Mandrioli,[9] A. Margotti,[9] V. Mascagna,[1,16] N. Mauri,[9] L. Meazza,[1,2] A. Meregaglia,[12] M. Mezzetto,[5] M. Nessi,[18] A. Paoloni,[20] M. Pari,[5,6] E. G. Parozzi,[1,2] L. Pasqualini,[9,19] G. Paternoster,[3] L. Patrizii,[9] M. Pozzato,[9] M. Prest,[1,16] F. Pupilli,[5] E. Radicioni,[8] C. Riccio,[10,11] A. C. Ruggeri,[10,11] C. Scian,[5,6] G. Sirri,[9] M. Stipćevic,[13] M. Tenti,[9] F. Terranova,[1,2] E. Vallazza,[1] F. Velotti,[18] M. Vesco[5,6] and L. Votano[20]

[1] *INFN Sezione di Milano-Bicocca, Piazza della Scienza 3, 20133 Milano, Italy*
[2] *Università di Milano-Bicocca, Piazza della Scienza 3, 20133 Milano, Italy*
[3] *Fondazione Bruno Kessler (FBK), Via Sommarive 18, 38123 Povo (TN), Italy*
[4] *INFN-TIFPA, Università di Trento, Via Sommarive 14, 38123 Povo (TN), Italy*
[5] *INFN Sezione di Padova, via Marzolo 8, 35131 Padova, Italy*
[6] *Università di Padova, via Marzolo 8, 35131 Padova, Italy*
[7] *INFN, Laboratori Nazionali di Legnaro, Viale dell'Università 2, 35020 Legnaro (PD), Italy*
[8] *INFN Sezione di Bari, Via Giovanni Amendola 173, 70126 Bari, Italy*
[9] *INFN Sezione di Bologna, viale Berti-Pichat 6/2, 40127 Bologna, Italy*
[10] *INFN, Sezione di Napoli, Strada Comunale Cinthia, 80126 Napoli, Italy*
[11] *Università "Federico II" di Napoli, Corso Umberto I 40, 80138 Napoli, Italy*
[12] *CENBG, Universitè de Bordeaux, CNRS/IN2P3, 33175 Gradignan, France*
[13] *Center of Excellence for Advanced Materials and Sensing Devices, Ruder Boskovic Institute, HR-10000 Zagreb, Croatia*
[14] *Institute of Nuclear Research of the Russian Academy of Science, 142190 Moscow, Russia*
[15] *INFN Sezione di Roma 1, Piazzale A. Moro 2, 00185 Rome, Italy*
[16] *Università degli Studi dell'Insubria, Via Valleggio 11, 22100 Como, Italy*
[17] *Università degli Studi di Bari, Via Giovanni Amendola 173, 70126 Bari, Italy*
[18] *CERN, Esplanade des Particules, 1211 Genève 23, Switzerland*
[19] *Università degli Studi di Bologna, viale Berti-Pichat 6/2, 40127 Bologna, Italy*
[20] *INFN, Laboratori Nazionali di Frascati, via Fermi 40, 00044 Frascati (Rome), Italy*
[*] *marta.torti@mib.infn.it*

Received 19 March 2020
Accepted 6 November 2020
Published 18 December 2020

*Corresponding author.

The knowledge of the initial flux, energy and flavor of current neutrino beams is the main limitation for a precise measurement of neutrino cross-sections. The ENUBET ERC project is studying a facility based on a narrow-band neutrino beam capable of constraining the neutrino fluxes normalization through the monitoring of the associated charged leptons in an instrumented decay tunnel. In ENUBET, the identification of large-angle positrons from K_{e3} decays at single particle level can potentially reduce the ν_e flux uncertainty at the level of 1%. This setup would allow for an unprecedented measurement of the ν_e cross-section at the GeV scale. This input would be highly beneficial to reduce the budget of systematic uncertainties in the next long baseline oscillation projects. Furthermore, in narrow-band beams, the transverse position of the neutrino interaction at the detector can be exploited to determine *a priori* with significant precision the neutrino energy spectrum without relying on the final state reconstruction. This contribution will present the advances in the design and simulation of the hadronic beam line. Special emphasis will be given to a static focusing system of secondary mesons that can be coupled to a slow extraction proton scheme. The consequent reduction of particle rates and pile-up effects makes the determination of the ν_μ flux through a direct monitoring of muons after the hadron dump viable, and paves the way to a time-tagged neutrino beam. Time-coincidences among the lepton at the source and the neutrino at the detector would enable an unprecedented purity and the possibility to reconstruct the neutrino kinematics at source on an event-by-event basis. We will also present the performance of positron tagger prototypes tested at CERN beamlines, a full simulation of the positron reconstruction chain and the expected physics reach of ENUBET.

Keywords: Neutrinos; neutrino beam; calorimeter.

PACS numbers: 29.40.−n, 29.90.+r

1. Introduction

Over the last 50 years, accelerator neutrino beams[1] have been developed toward higher intensities, but uncertainties in the flux and in the flavor composition are still very large. Thanks to the progress in neutrino scattering experiments,[2,3] the measurements of neutrino cross-sections are now limited by the knowledge of the initial fluxes, since the yield of neutrinos is not directly measured but it is extrapolated from hadro-production data and detailed simulations of the neutrino beamline. This limitation bounds the precision that can be reached in the measurement of the absolute cross-sections to $\mathcal{O}$(5–10%). Moreover, pion-based sources mainly produce ν_μ while most of the next generation oscillation experiments will rely on the appearance of ν_e at the far detector. In fact, a direct measurement of the ν_e cross-sections is of great interest for the current (T2K, NOνA) and next (DUNE, HyperK) generation of oscillation experiments.[4]

These considerations motivated the development of "monitored" neutrino beams[5] and the Enhanced NeUtrino BEams from kaon Tagging (ENUBET) proposal:[6] a neutrino beam facility where the dominant source of electron neutrino contamination is the three body semileptonic decay of the kaons $K^+ \to \pi^0 e^+ \nu_e$ (K_{e3}), in which the electron neutrino flux is monitored directly by the observation of large-angle positrons in the decay tunnel.

The ERC ENUBET ("Enhanced NeUtrino BEams from kaon Tagging") project[7] is aimed at building a detector capable of identifying positrons from K_{e3} decays

while operating in the harsh environment of a conventional neutrino beam decay tunnel. Since March 2019, ENUBET is also a CERN Neutrino Platform project (NP06/ENUBET) developed in collaboration with CERN A&T and CERN-EN.

The ENUBET neutrino beam is a conventional narrow-band beam with a short ($\sim$20 m) transfer line followed by a 40 m long decay tunnel. Particles produced by the interaction of protons on the target are focused, momentum selected and transported at the entrance of the tunnel, as described in Sec. 2. The particles that reach the decay tunnel are hence pions, kaons and protons within the momentum bite of the transfer line (10% in ENUBET). Off-momentum particles are mostly low energy pions, electron, positron and photons from tertiary interactions in the collimators and other components of the beamline, and muons from pion decay that cross the collimators. The rates of these particles are several orders of magnitude smaller than beams currently in operation and particle creation in the decay tunnel can be monitored at single particle level by instrumenting a fraction of the decay tunnel.

Three different prototypes were built and tested at CERN PS East Area in order to select the appropriate layout for the tagger demonstrator: two prototypes are shashlik-based calorimeters (see Sec. 3) while the third one was built with lateral scintillation light readout (see Sec. 4).

Particles identification is performed by a Neural Network approach based on a Multivariate Data Analysis as described in Sec. 5.

ENUBET will provide a precise measurement of ν_e and ν_μ fluxes and exploit correlation between the radial position of the neutrino interaction and its energy, as described in Sec. 6.

Finally, ENUBET aims at to set the first milestone toward a "time-tagged neutrino beam," where the ν_e at the detector is time-correlated with the produced e^+ in the decay tunnel, as we will see in Sec. 7.

2. The ENUBET Beamline

The ENUBET beam is a conventional narrow-band beam with two differences with respect to the current beams: the decay tunnel is not located along the proton axis of the focusing system and the proton extraction length is slow ($\mathcal{O}(s)$). Particles produced by proton interactions in the target are focused, momentum selected and transported to the tunnel entrance. Noninteracting protons are stopped in a proton beam dump. Off-momentum particles reaching the decay tunnel are mostly low energy particles coming from interactions in the collimators and other beamline components together with muons that cross absorbers and collimators. The hadron beam considered has a reference momentum of 8.5 GeV/c with a momentum bite of 10% and we expect $\sim$50% of K^+ to decay in a 40 m long tunnel.

ENUBET goals can be achieved using conventional magnets by maximizing the number of K^+ and π^+ at tunnel entrance, by minimizing the total length of the transfer line to reduce kaon decay losses and by keeping under control the level of

Table 1. Expected π^+ and K^+ for proton on target (PoT) at the decay tunnel entrance for the two possible focusing schemes. The improvement factor in kaon transport with respect to Ref. 5 is shown in the last column.

Focusing	π/PoT $[10^{-3}]$	K/PoT $[10^{-3}]$	Extraction length	π/cycle (10^{10})	K/cycle (10^{10})	Factor with respect to Ref. 5
Horn-based	97	7.9	2 ms	438	36	$\times$ 2
Static	19	1.4	2s	85	6.3	$\times$ 4

background transported. Momentum and charge-selected hadrons $\left(K^+, \pi^+\right)$ being injected in the instrumented decay tunnel, need to be collimated enough such that any undecayed meson is capable of escaping the region without hitting the tagger inner surface: this limits the particles rate at the instrumentation.

Primary proton interactions in the target are simulated with FLUKA,[8] considering various proton drivers (400 GeV, 120 GeV and 30 GeV protons) and target designs (Be or Graphite). The results reported in this document refer to 400 GeV protons and a Be target 110 cm long with a 3 mm diameter. The optic optimization is performed with TRANSPORT[9] to match the ENUBET specifications for momentum bite and beam envelope. The beam components and lattice are then implemented in G4Beamline[10] that fully simulates particle transport and interactions.

Two possible beamlines have been considered: the first one makes use of a focusing horn placed between the ENUBET target and the following transfer line ("horn-based transfer line") while in the second one the transfer line quadrupoles are placed directly downstream the target ("static transfer line"). The performances of the static design, as shown in Table 1, turned out to be better than early estimates reported in the ENUBET proposal[5] and it offers several advantages in terms of cost, simplification of technical implementation and performance of particle identification.[11]

2.1. *Static transfer line*

The static configuration allows to perform the focusing using DC operated devices (unlike pulsed magnetic horns) compatible with a traditional slow extraction of several seconds.

The best configuration (see Fig. 1) consists in a quadrupole triplet followed by a dipole that provides a 7.4° bending angle and by another quadrupole triplet.

The rate of background particles is several orders of magnitude smaller than present beams and the instrumentation located in the decay tunnel can monitor lepton production at single particle level. Figure 2 shows the momentum distribution and the XY profile of K^+ entering/exiting the decay tunnel.

The length of the decay tunnel is optimized in order to have K_{e3} decays as the dominant ν_e source: electron neutrinos from decay in flight of kaons represent

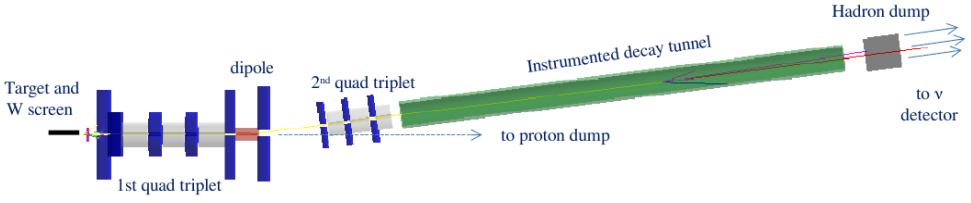

Fig. 1. Schematics of the ENUBET beam in the static focusing option.

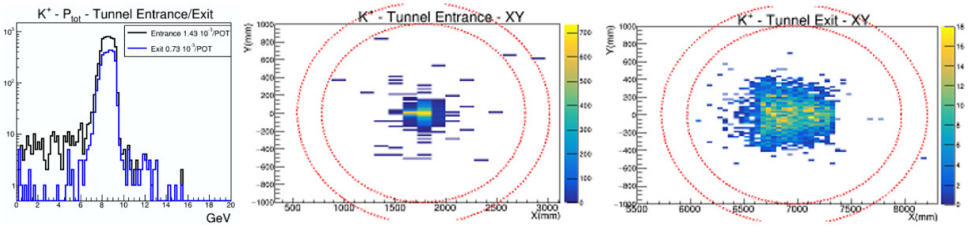

Fig. 2. (Color online) Left: momentum distribution of K^+ entering (black)/exiting (blue) the decay tunnel. Middle: XY profile of the K^+ beam at tunnel entrance. Right: XY profile of the K^+ beam at tunnel exit.

$\sim 97\%$ of the overall ν_e flux. Positrons from three body decays are emitted at large angles and hit the instrumented walls of the tunnel before exiting.

The static beamline transports at the tunnel entrance $19 \times 10^{-3}\pi^+$/PoT and $1.4 \times 10^{-3}K^+$/PoT in $[6.5 \div 10.5$ GeV/$c]$ range, improving by four times the kaon yield with respect to the first estimate reported in Ref. 5 and requiring about 4.5×10^{19} PoT at CERN SPS to carry out both ν_μ and ν_e cross-section programs. An additional advantage of the static solution is the possibility to directly monitor the rate of muons from π^+ decays after the hadron dump: the reduced yield with respect to the horn-based solution and the consequent lower particle rate allow for a monitoring of the ν_μ flux at single particle level.

3. Instrumentation of the Decay Tunnel

The positron monitoring is achieved instrumenting the decay tunnel. The requirements for the detector are: a high e/π separation capability to remove the main source of background; radiation hardness, since it will operate in a harsh environment; cost effectiveness, since a large fraction of the decay tunnel will be instrumented; fast recovery time to cope with the expected rate of 200 kHz/cm^2. These requirements are fullfilled by a sampling calorimeter with a longitudinal segmentation for positron tagging complemented by a photon veto, in order to discriminate neutral pions and gammas. A shashlik calorimeter[12,13] with longitudinal segmentation was identified as a solution for the ENUBET requirements.

The final layout of the tagger will be composed by three calorimeter layers and equipped by the photon veto.

3.1. *Shashlik prototype*

The first shashlik prototype was composed by five, 15 mm thick, iron layers interleaved by 5 mm thick plastic scintillator tiles.[14,15] The total length of the module (10 cm) and its transverse size (3×3 cm^2) correspond to 4.3 X_0 and 1.7 Moliere radii, respectively. Nine wavelength shifting (WLS) fibers crossing the UCM are connected directly to 1 mm^2 Silicon Photomultipliers (SiPMs) through a plastic holder. SiPMs are hosted on a PCB embedded in the calorimeter structure, as schematized in Fig. 3 (right).

In November 2016, a prototype consisting of a $7 \times 4 \times 2$ array of UCMs was exposed, at the CERN PS East Area facility, to beam composed by electrons, muons, and pions with momentum in the range of interest for neutrino physics applications (1–5 GeV), in order to measure its performances.[16]

The scintillator tiles were machined and polished from EJ-200 and BC-412 sheets and painted with a diffusive TiO_2 based coating (EJ-510) to increase the light collection efficiency. After painting, nine holes were drilled in each tile in order to accommodate the WLS fibers (Y11 and BCF92) read out by FBK 20 μm-pixel SiPMs.

Ancillary detectors were used to identify particle type and isolate samples of electrons and muons. During the data taking the calorimeter was tilted at different angles (0, 50, 100, 200 mrad) with respect to the beam direction. The tilted geometry reproduces the operating condition of the calorimeter in the decay tunnel of neutrino beams, where positrons from K^+_{e3} reach the detector with an average angle of ~ 100 mrad.

The measured deposited energy is in good agreement with the results obtained from a Monte Carlo simulation that took into account all the different components of the beam.

The electromagnetic energy resolution is well described by $\sim 17\%/\sqrt{E\ (\mathrm{GeV})}$ showing that the dominant contribution to the resolution is due to the sampling term and that the energy response is not affected by the light readout scheme employed to achieve longitudinal segmentation. A good e/π separation, with a pion misidentification lower than 3%, is achieved exploiting the longitudinal segmentation of the calorimeter and the different energy deposit patterns.

Furthermore, the analysis of the tilted runs indicates that the performance of the calorimeter is similar to the 0 mrad run in the angular range of interest for ENUBET. Finally, the calorimeter shows linear response, within $< 3\%$, in the whole range of interest in both standard (0 mrad) and tilted runs.

The integration of the light readout into the calorimeter module is a very effective solution but results in exposing the SiPMs to fast neutrons produced by hadronic showers. In order to evaluate the effect of the radiation on the performances of the SiPMs, three PCBs hosting 9 SiPMs and the single-SiPM PCB were irradiated from a minimum dose of 1.8×10^8 n/cm^2 up to 1.7×10^{11} n/cm^2 at the irradiation facility of INFN-LNL (Laboratori Nazionali di Legnaro).

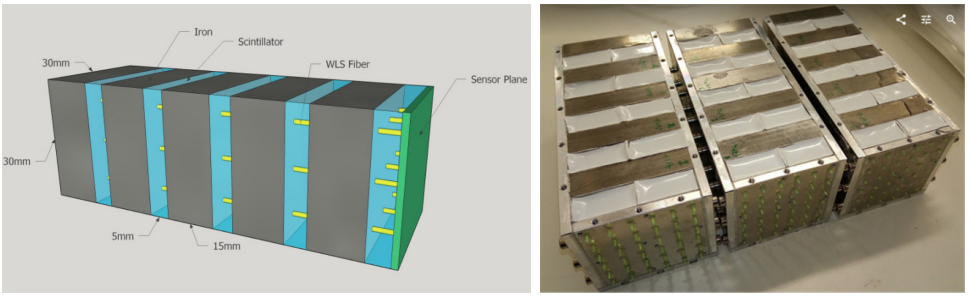

Fig. 3. Left: scheme of the baseline shashlik UCM. Right: pictures of the polysiloxane-based calorimeter prototype.

All the SiPMs show minor changes in the breakdown voltage, while the dark current after breakdown increases by more than two orders of magnitude at a fluence of $\sim 10^{11}$ n/cm^2. Finally, the sensitivity to single photoelectron is lost at fluences larger than 3×10^9 n/cm^2.

The irradiated PCBs were then installed in two calorimeter prototypes and tested at CERN: the electron and mip peak mean value ratio is constant after irradiation and the integrated neutron fluence does not affect the dynamic range of the photosensors.[17]

3.2. *The polysiloxane prototype*

Nonconventional options based on polysiloxane scintillators are also being examined. Polysiloxane is a siliconic-based scintillator[18] that offers several advantages over plastic scintillators: better radiation tolerance, reduced aging, no irreversible deterioration caused by mechanical deformations, exposure to solvent vapors and high temperatures and, for shashlik calorimeters, no need to drill and insert the optical fibers. Silicone rubbers preserve their transparency even after a 10 kGy dose exposure and their physical properties are constant over a wide temperature range. Polysiloxane can be poured at 60°C in the shashlik module after the insertion of the optical fibers in the absorber, simplifying the assembly. On the other hand, the light yield is about 30% of the EJ-200 yield.

A polysiloxane shashlik calorimeter prototype (Fig. 3 (right)) composed of three modules ($6 \times 6 \times 15$ cm^3 each, 13 X_0 in total) consisting of 12 UCM units and with a 15 mm scintillator tile thickness was built and exposed to particle beams at the CERN East Area in October 2017.[19]

An electromagnetic energy resolution of $\sim 17\%/\sqrt{E\ (\mathrm{GeV})}$ and good linearity ($< 3\%$ in the 1–5 GeV range) were measured.

4. Design and Test for the Lateral Scintillation Light Readout Prototype

The shashlik option has two disadvantages: SiPMs suffer large radiation levels lying within the calorimeter bulk and they are not accessible for maintenance during the

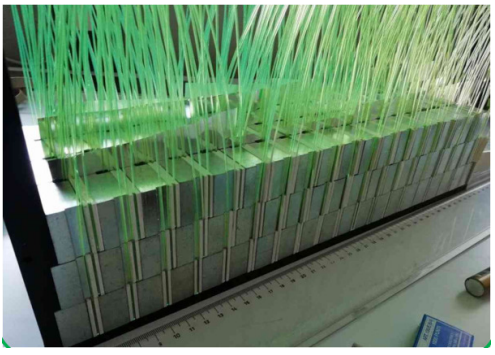

Fig. 4. Pictures of the lateral scintillation light readout calorimeter prototype.

data taking. For this reason we implemented a different solution for the scintillation light readout.

The current design consists in a scheme where light is collected from both sides of each scintillator tile through WLS fibers installed in grooves machined on the plastic. This setup replaces the shashlik-based UCM with a Lateral readout Compact Module (LCM) in which fibers from the same LCM are bundled to a single SiPM reading in groups of 10 at a distance of about 30 cm from the bulk of the calorimeter.

In this layout SiPMs are not embedded in the calorimeter bulk, thus not exposed to the shower, and this setup allows for an easier access regarding maintenance or replacements.

In fact, FLUKA simulations[20] demonstrate that placing SiPM above 30 cm of borated polyethylene, can reduce the neutron flux on the sensors by a factor 18.

In 2018, a prototype made of $3 \times 2 \times 2$ LCM was assembled as shown in Fig. 4. Each LCM was composed of 1.5 cm thick iron slabs interleaved with 0.5 cm plastic scintillators (EJ-204): the modules thus have the same sampling fraction as the shashlik UCM.

The prototype was tested at CERN at the T9 beamline in May 2018. Later, in September, a larger prototype consisting of 84 LCMs in the $7 \times 4 \times 3$ structure was exposed to CERN SPS beam.

As for the previous prototypes, during the test beam the calorimeter was tilted at different angles (0, 50, 100, 200 mrad) with respect to the beam direction and exposed to electrons, pions and muons. These particles were identified thanks to ancillary detectors present in the experimental area. The test beam results were compared with a Monte Carlo simulation. The calorimeter response to minimum ionizing particles, electrons and pions was evaluated and showed a good agreement with the prediction for the energy range 1–3 GeV. Preliminary results showed an electromagnetic energy resolution at 1 GeV of about 17% which is consistent with the prediction. In addition, data and prediction mutually agreed with a linear response in the range 1–3 GeV. The analysis of test beam data is still ongoing.[20]

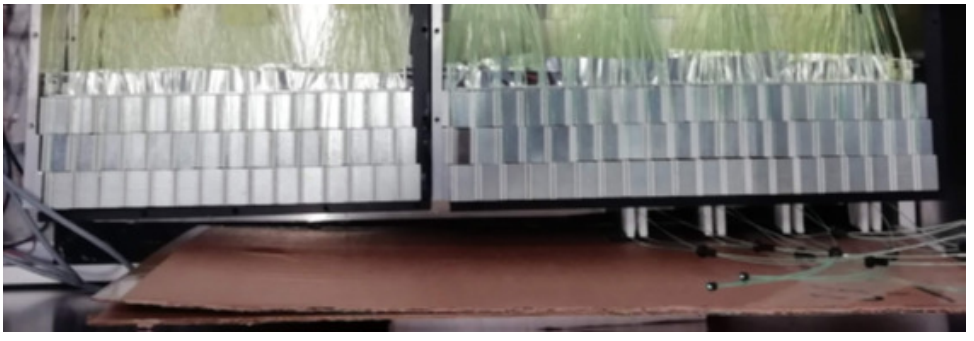

Fig. 5. Four doublets of the photon veto installed below the lateral readout prototype during the September 2018 test at CERN. The t_0 layer is visible in the bottom right side of the picture.

4.1. *The photon veto*

Photons originating from $K^+ \to \pi^+ \pi^0 (K_{\pi 2})$ decays and reaching the positron tagger[5] must be discriminated from positrons by a suitable photon veto (t_0 layer). This detector also provides coarse information on the impact point of the particle and timing information. In the baseline option for the t_0 layer the basic unit is a doublet of plastic scintillator tiles with a $\sim 3 \times 3$ cm^2 surface and a 0.5 cm thickness ($\sim 0.02\ X_0$), readout by a WLS fiber optically linked to a SiPM. The doublets are orthogonal to the tagger axis and mounted below the inner radius of the calorimeter. Adjacent tiles form a ring installed inside the positron tagger. Along the z-axis, t_0 layer rings are separated by 7 cm to have on average about five hit doublets for K_{e3} positrons. Photon conversions are discriminated from positrons using the information on the pulse height in all hit scintillators. Photon converted in the photon veto are rejected requiring a signal compatible with a single mip (1–2 mip separation).

The t_0 layer was tested in stand alone configuration and, in September 2018, coupled with the calorimeter (see Fig. 5) during the test beam at CERN. Data analysis is ongoing.[20]

5. Particle Reconstruction

Positron identification has been simulated starting from particles transported by the ENUBET beamline at the entrance of the decay tunnel. The ENUBET GEANT4[21–23] simulation includes particle tracking and detector response and the full particle identification (PID) chain from the event builder to the positron identification. PID is based on a Multivariate Data Analysis (MTVA) that employs variables constructed from the energy deposit in each module.

The first step needed for PID is the definition of the event by the ENUBET Event Builder (EB).

In the standard positron identification analysis,[24,25] all the modules of the first e.m. layer in which an energy deposition is found, are ordered in time and the first

available UCM with a visible energy larger than 20 MeV is selected as the seed of the event. UCM and t_0 signals close in time and space to the seed one are clustered to build the event. The procedure is iterated over all the recorded signals.

Charged particles will deposit energy in different UCMs and the geometrical pattern of the energy deposition can be exploited to perform particle identification. Indeed positrons will produce showers well contained in the first two calorimeter layers and in few UCMs along the longitudinal coordinate, whereas pions will have a less compact shower and a larger fraction of energy deposited in the third layer.

To exploit the calorimeter information as much as possible, we used a Neural Network (NN) based on TMVA multivariate analysis. In particular we used variables such as the fraction of energy in the first e.m. layer, the fraction in the event seed and several others containing information on the shower profile development. To further improve the background rejection, the longitudinal distribution of the events along the tunnel is also used, since the signal is more abundant in the second part of the tunnel due to its geometrical acceptance.

The NN analysis allows to separate positrons from pions and muons but does not remove the contamination of photons from π^0 decays. The e^+/γ separation is performed using the signal of the t_0 layer. Looking at the energy deposited in the two layers of the doublet we can discriminate between zero, one or two mip selecting positrons and rejecting photons converting in the first t_0 layer.

This analysis chain allows to select positrons with a signal-to-noise ratio of ~ 0.5 and an efficiency of $\sim 20\%$, which is appropriate for the neutrino flux monitoring at the percent level. This level of reconstruction is achieved for the static focusing system described before. A recent tuning in the beamline design and the reconstruction algorithms improve these figures significantly.

6. The ENUBET Narrow-Band Beam

ENUBET physics program can be enhanced by two additional features: provide a beam with a precisely measured flux and a measurement of the neutrino energy that does not rely on the reconstruction of final state particles (narrow-band off-axis technique).[26]

In fact, the monitoring of positrons in the decay tunnel provides the ν_e flux, while the slow extraction scheme allows for a high precision ν_μ flux measuring the muons rate after the hadron dump. Neutrino fluxes were estimated simulating samples of positive pions and kaons with a momentum bite of 10% centered at 8.5 GeV/c, considering the static transfer line with 400 GeV protons and a liquid argon detector placed at 90 m from the entrance of the decay tunnel. Collecting data for about 1 year of SPS operations (4.5×10^{19} PoT), at the neutrino detector about 1.13×10^6 ν_μ CC and 1.4×10^4 ν_e interactions will be observed.

The narrow-band off-axis technique results from the narrow momentum bandwidth of the beam and the finite transverse dimension of the neutrino detector. The energy measurement exploits the correlation between the energy of the neutrino

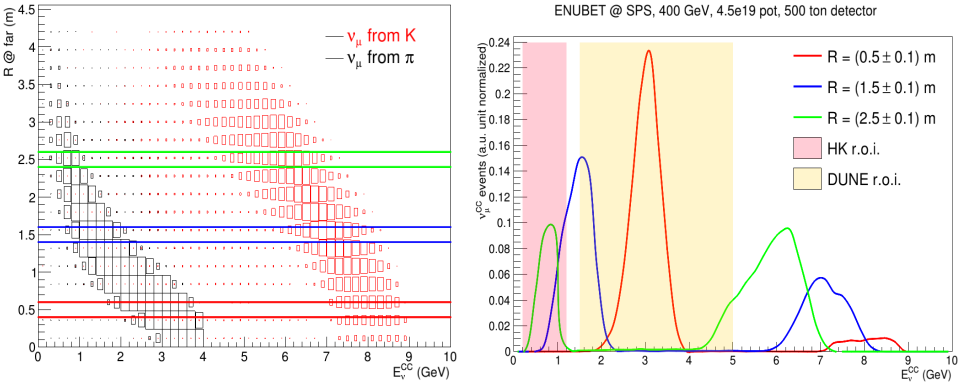

Fig. 6. (Color online) Left: Radial and energy distribution of ν_μ CC interactions. The high energy neutrino component from kaon decays is shown with red boxes, while the low energy one is reported with black boxes. Right: ν_μ CC spectra normalized to unity obtained selecting interactions at different radial distances from the beam axis. Region of interest for future long baseline experiments are enlightened.

interacting in the detector and the radial distance R of the interaction vertex from the beam axis (Fig. 6 (left)). As shown in Fig. 6 (right), it is possible to collect ν_μ CC event samples covering the energy range of interest for future long baseline oscillation experiments, selecting interaction in radial windows of $R \pm 10$ cm.

The incoming neutrino energy is determined with a precision given by the pion peak width of the spectrum at a fixed R as shown in Fig. 7. Only a rough cut on the visible energy is needed to separate the ν_μ from pion decay from the ν_μ originating from the two-body kaon decay. In this way, differential cross-section measurements can be performed without relying on the reconstruction of the final state products for the determination of the neutrino energy. Absolute ν_μ cross-section

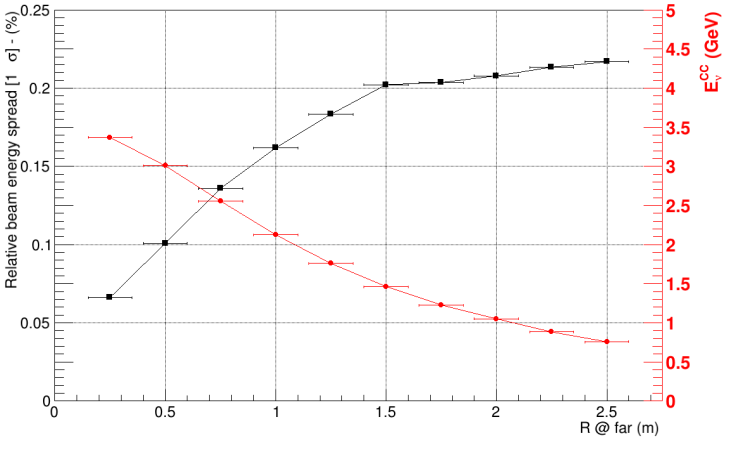

Fig. 7. (Color online) Beam energy spread (in black) and peak energy (in red) as a function of the distance R of the interaction vertex at the neutrino detector from the beam axis.

measurements can be performed by combining the narrow-band off-axis technique with the measurement of the ν_μ flux from pion decay during the extraction. The flux measurement can be exploited using scintillators located after the hadron dump. Studies on this possibility are ongoing.

7. From Monitored to Tagged Neutrino Beam

A purely static focusing system opens up several opportunities beyond the original goals of ENUBET. Since in the static focusing system the proton extraction can last up to several seconds, the instantaneous rates of particles hitting the decay tunnel walls are reduced by about two orders of magnitude compared with the horn option.

In the ENUBET static option the time between two K_{e3} decays is 11.3 ns. A neutrino interaction in the detector can thus be time linked with the observation of its associated lepton in the decay tunnel, giving a "tagged neutrino beam."[28–32] In order to suppress accidental coincidences between the neutrino interaction and uncorrelated particles inside the beam pipe, the timing precision of the detectors that are used to instrument the decay tunnel must reach 100 ps. This precision is needed also to associate the positron with the other decay products of the kaons.[33] The physics potential of tagged neutrino beams is enormous because they provide energy and flavor measurement on event-by-event basis and are the ideal tools to study cross-sections and nonstandard oscillation phenomena, including sterile neutrinos. R&D on the photon tagger and the neutrino detector to bring the required time resolution have been started.

8. Conclusions

During the first years of activities, ENUBET has achieved important milestones and extended remarkably its physics case. The R&D carried out includes the design of the transfer line and the tests of the prototypes at the CERN East Area. The project is aimed at delivering a complete design of the ENUBET beamline by 2021. Beyond ν_e cross-section measurements, the ENUBET physics potential is being investigated for the study of ν_μ interaction and the determination of differential cross-sections employing the narrow-band off-axis technique. The static focusing system opens up the possibility of transforming ENUBET in the world first tagged neutrino beam and the corresponding technical challenges are being addressed.

Acknowledgments

This project has received funding from the European Union's Horizon 2020 Research and Innovation program under Grant Agreement No. 681647 and by the Italian Ministry of Education and Research — MIUR (Bando "FARE," progetto NuTech). It is also supported by the Department of Physics "G. Occhialini," University of Milano-Bicocca (project 2018-CONT-0128).

References

1. S. E. Kopp, *Phys. Rep.* **439**, 101 (2007).
2. T. Katori and M. Martini, *J. Phys. G* **45**, 013001 (2018).
3. L. Alvarez-Ruso *et al.*, *Prog. Part. Nucl. Phys.* **100**, 1 (2018).
4. A. M. Ankowski and C. Mariani, *J. Phys. G* **44**, 054001 (2017).
5. A. Longhin, L. Ludovici and F. Terranova, *Eur. Phys. J. C* **75**, 155 (2015).
6. A. Berra *et al.*, CERN-SPSC-2016-036, SPSC-EOI-014, Geneva, 2016.
7. F. Acerbi *et al.*, CERN-SPSC-2018-034, SPSC-I-248, Geneva, 2018.
8. A. Fassò, A. Ferrari, J. Ranft and P. R. Sala, FLUKA: A multi-particle transport code, CERN-2005-10 (2005), INFN/TC-05/11, SLAC-R-773.
9. D. C. Carey, K. L. Brown and F. Rothacher, SLAC-R-95-462, Stanford, 1995.
10. T. J. Roberts, K. B. Beard, D. Huang, S. Ahmed, D. M. Kaplan and L. K. Spentzouris, *Conf. Proc. C* **WEPP120**, 0806233 (2008).
11. G. Brunetti *et al.*, arXiv:1903.09044.
12. H. Fessler, P. Freund, J. Gebauer, K. M. Glas, K. Pretzl, P. Seyboth, J. Seyerlein and J. C. Thevenin, *Nucl. Instrum. Methods A* **228**, 303 (1985).
13. G. S. Atoian *et al.*, *Nucl. Instrum. Methods A* **320**, 144 (1992).
14. A. Berra *et al.*, *Nucl. Instrum. Methods A* **830**, 345 (2016).
15. A. Berra *et al.*, *IEEE Trans. Nucl. Sci.* **64**, 1056 (2017).
16. G. Ballerini *et al.*, *J. Instrum.* **13**, P01028 (2018).
17. F. Acerbi *et al.*, *J. Instrum.* **14**, P02029 (2019).
18. A. Quaranta *et al.*, *J. Non-Cryst. Solids* **357**, 1921 (2011).
19. F. Acerbi *et al.*, *Nucl. Instrum. Methods A* **956**, 163379 (2020).
20. F. Acerbi *et al.*, *J. Instrum.* **15**, P08001 (2020).
21. S. Agostinelli *et al.*, *Nucl. Instrum. Methods A* **506**, 250 (2003).
22. J. Allison *et al.*, *IEEE Trans. Nucl. Sci.* **53**, 270 (2006).
23. J. Allison *et al.*, *Nucl. Instrum. Methods A* **835**, 186 (2016).
24. A. Meregaglia, Talk at *30th Rencontres de Blois*, Blois, 3–8 June 2018.
25. F. Pupilli, *PoS* **NEUTEL2017**, 078 (2018).
26. F. Pupilli, *PoS* **NOW2018**, 030 (2018).
27. L. N. Hand, *Proceedings of Second NAL Summer Study*, Aspen, Colorado, 9 June–3 August 1969.
28. B. Pontecorvo, *Lett. Nuovo Cimento* **25**, 257 (1979).
29. P. Denisov *et al.*, preprint IHEP 81-98, Serpukhov, 1981.
30. R. H. Bernstein *et al.*, FERMILAB-Proposal-0788, 1989.
31. L. Ludovici and P. Zucchelli, arXiv:hep-ex/9701007.
32. L. Ludovici and F. Terranova, *Eur. Phys. J. C* **69**, 331 (2010).
33. F. Acerbi *et al.*, Input document for the European Particle Physics Strategy, arXiv:1901.04768 [physics.ins-det].